Multistage symmetry breaking in the breathing pyrochlore lattice Li(Ga,In)Cr_{4}O_{8}

S. Lee, S.-H. Do, W.-J. Lee, Y. S. Choi, M. Lee, E. S. Choi, A. P. Reyes, P. L. Kuhns, A. Ozarowski, and K.-Y. Choi

Multistage symmetry breaking in the breathing pyrochlore lattice Li(Ga,In)Cr$_4$O$_8$

S. Lee,[1] S.-H. Do,[1] W.-J. Lee,[1] Y.S. Choi,[1] M. Lee,[2, 3] E. S. Choi,[3]

A. P. Reyes,[3] P. L. Kuhns,[3] A. Ozarowski,[3] and K.-Y. Choi[1, *]

[1]*Department of Physics, Chung-Ang University, Seoul 156-756, Republic of Korea*

[2]*Department of Physics, Florida State University, Tallahassee, Florida 32306, USA*

[3]*National High Magnetic Field Laboratory,*

Florida State University, Tallahassee, Florida 32310, USA

(Dated: April 6, 2016)

Abstract

We present magnetic susceptibility, dielectric constant, high-frequency electron spin resonance, ^{7}Li nuclear magnetic resonance, and zero-field muon spin relaxation measurements of LiACr$_4$O$_8$ (A=Ga, In), towards realizing a breathing pyrochlore lattice. Unlike the uniform pyrochlore ZnCr$_2$O$_4$ lattice, both the In and Ga compounds feature two-stage symmetry breaking: a magnetostructural phase transition with subsequent antiferromagnetic ordering. We find a disparate symmetry breaking process between the In and Ga compounds, having different degrees of bond alternation. Our data reveal that the Ga compound with moderate bond alternation shows the concomitant structural and magnetic transition at $T_S = 15.2$ K, followed by the magnetic ordering at $T_m = 12.9$ K. In contrast, the In compound with strong bond alternation undergoes a thermal crossover at $T^* \approx 20.1$ K from a tetramer singlet to a dimer singlet or a correlated paramagnet and a separate weak magnetostructural transition at $T_S = 17.6$ K and the second antiferromagnetic ordering at $T_m = 13.7$ K. This suggests that the magnetic phases and correlations of the breathing pyrochlore lattice can be determined from the competition between the bond alternation and spin-lattice coupling, thus stabilizing long-range magnetic ordering against a nonmagnetic singlet.

I. INTRODUCTION

Magnetic frustration and competing interactions are key concepts in modern condensed matter physics. This is due to the potential to observe exotic states of matter with unconventional low-lying excitations and quantum criticality[1,2]. Spinel oxides AB_2O_4 are a particularly appealing example of an octahedral B site forming a three-dimensional (3D) network of corner-sharing tetrahedra, i.e., a pyrochlore lattice[3,4]. The pyrochlore antiferromagnet hosts a variety of novel emergent phenomena such as zero-energy excitations, field-induced phase transitions, and diverse ordered phases[5,6]. These are related to a macroscopic degeneracy of classical ground states and a lift of ground-state degeneracies through thermal and quantum fluctuations, spin-lattice couplings, and spin exchange processes[7–12]. Along with these phenomena, a magnetic ordering process can also be controlled by introducing alternating lattice distortions.

The breathing pyrochlore system, which consists of an alternating array of small (S) and large (L) tetrahedra, embodies bond alternation and frustration in a single material as shown in Fig. 1(a)[13–19]. Its spin Hamiltonian is given by $\mathcal{H} = J \sum_{ij\in S} \mathbf{S}_i \cdot \mathbf{S}_j + J' \sum_{ij\in L} \mathbf{S}_i \cdot \mathbf{S}_j$ with nearest-neighbor exchange interaction J for the S-tetrahedra and J' for the L-tetrahedra. The magnetic phase of the breathing pyrochlore lattice is determined by the breathing parameter $B_f = J'/J$. The end members are an isolated tetrahedron with $B_f = 0$ and a uniform pyrochlore with $B_f = 1$. The ground states are a tetramer singlet and spin liquid, respectively[20,21]. However, little is known about the magnetic phases in the intermediate parameter range of $0 < B_f < 1$.

The A-site ordered $LiACr_4O_8$ (space group $F\bar{4}3m$) spinels realize the breathing pyrochlore system with $B_f = 0.6$ for A=Ga and 0.1 for A=In[13], thus providing a promising platform for studying the combined effect of frustration and bond alternation. These compounds are derived from the widely investigated Cr-based ACr_2O_4 spinels. The A-site ordering originates from the large difference in the valence states between Li^+ and Ga^{3+}/In^{3+}. Similarly to the uniform pyrochlore counterparts of ACr_2O_4, magnetostructural ordering occurs through spin-lattice coupling at 15.5 K for A=Ga and 16 K for A=In[13]. The magnetic susceptibility of $LiGaCr_4O_8$ resembles that of $ZnCr_2O_4$. ^7Li NMR measurements evidenced a first-order antiferromagnetic transition with a critical divergence of the nuclear spin-lattice relaxation rate, $1/T_1$, toward 12.8 K, suggesting proximity to a tricritical point[14]. In comparison with

the Ga compound, both the magnetic susceptibility and NMR data of $LiInCr_4O_8$ show a spin-gap behavior of $\Delta = 31-57$ K in the high-temperature cubic phase, signaling dominant singlet correlations[13,14]. A recent neutron diffraction study of the In compound disclosed that the structural transition accompanies a weak magnetic order with the subsequent magnetic long-range order at $T_m = 12.9$ K[16,22]. In spite of the substantial difference in B_f, the Ga and In compounds seem to share a two-stage symmetry lowering process. However, when substituting Ga for In, $LiInCr_4O_8$ is not smoothly interconnected to $LiGaCr_4O_8$[15]. Instead, for both compounds, the magnetic ordering is rapidly suppressed upon introducing a small amount of Ga or In. This implies the distinct evolution of magnetic correlations between the Ga and In compounds, calling for further investigations.

In this paper, we employ multiple magnetic resonance techniques to elucidate the role of breathing lattice distortions in creating the two-step magnetic transition in $LiACr_4O_8$. We find that the Ga compound is characterized by a concomitant magnetic and structural transition with subsequent magnetic ordering. This is contrasted by the In compound, in which a thermal crossover proceeding the magnetostructural and magnetic transitions occurs from a tetramer singlet to a dimer singlet or a correlated paramagnet. The precursor transition of $LiInCr_4O_8$ signifies the competing role of bond alternation and spin-lattice coupling in relieving degeneracy.

II. EXPERIMENTAL DETAILS

Polycrystalline samples of $LiACr_4O_8$ were synthesized by the conventional solid-state reaction method as described in Ref.[13]. For dielectric constant measurements, $LiGaCr_4O_8$ ($LiInCr_4O_8$) samples were cut into a plate shape with an area of 7.2 mm^2 (13.0 mm^2) and thickness of 0.11 mm (0.38 mm). Contacts were made on each plate face with silver paint. An AC electric field with 136 kV/m and 40 kV/m for the Ga and In samples, respectively, at various frequencies were applied. A commercial capacitance bridge (Andeen-Hagerling, AH2700A model) was used to measure the capacitance and dissipation of the samples. The dielectric constant was then calculated on the assumption that the samples are an ideal infinite parallel plate.

High-frequency electron spin resonance (ESR) experiments were carried out at $\nu = 328.8$ GHz using the transmission spectrometer developed at the National High Magnetic

Field Laboratory (NHMFL) with a sweepable 15 T superconducting magnet. For ^{7}Li ($I = 3/2$, $\gamma_N/2\pi = 16.547$ MHz/T) nuclear magnetic resonance (NMR) measurements, we employed a locally developed NMR spectrometer in NHMFL equipped with a high homogeneity 17 T field-varying magnet. ^{7}Li NMR spectra were recorded by fast Fourier transform (FFT) of the NMR echo signal while sweeping the field at a fixed frequency of $\nu = 182.098$ MHz. The nuclear spin-lattice (spin-spin) relaxation time T_1 (T_2) was measured by a modified inversion recovery (Hahn pulse) method in the temperature range of $T = 3 - 200$ K.

Muon spin relaxation (μSR) experiments were performed on the EMU spectrometer at ISIS (Rutherford Appleton Laboraty, UK) and on the LAMPF spectrometer at TRIUMF (Vancouver, Canada). While the samples at ISIS were mounted on a silver backing plate, the specimens were wrapped with a silver foil and attached to the sample holder in TRIUMF. The mounted samples were then inserted into a cryostat with a temperature range of $1.6 - 300$ K. At ISIS, pulses of spin polarized muons were implanted into the sample with a full width at half maximum (FWHM) of 80 ns. In contrast, continuous muon sources in TRIUMF have no dominating time structure. Therefore, the advantage of the continuous muon beam is that it enables the observation of fast oscillations and fast relaxations in an initial time interval. The measured physical quantity is the evolution of the muon polarization $P_z(t)$ which is determined by

$$P_z(t) = \frac{N_B(t) - \alpha N_F(t)}{N_B(t) + \alpha N_F(t)} \tag{1}$$

where $N_F(\text{t})$ and $N_B(\text{t})$ are the muon counts at the detectors antiparallel and parallel to an incident muon spin direction, respectively, and α is the efficiency ratio between forward and backward detectors, which is determined from μSR experiments with transverse magnetic field (~ 50 Oe) in a paramagnetic state.

III. RESULTS

A. Magnetic susceptibility

The temperature dependence of the magnetic susceptibility $\chi(T)$ for LiACr$_4$O$_8$ is shown in Fig. 1(b). $\chi(T)$ of the In compound exhibits a round maximum at around 60 K and a subsequent exponential-like drop, indicative of the opening of a spin gap. The low-temperature up-
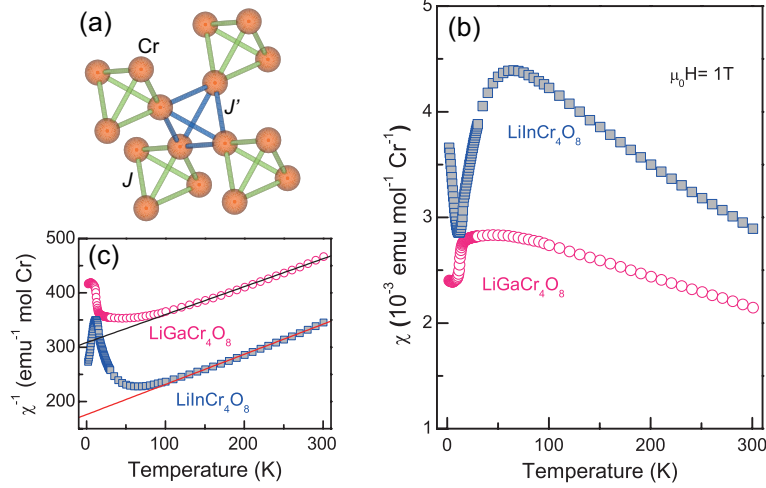
FIG. 1: (Color online) (a) Sketch of a breathing pyrochlore lattice. The two tetrahedra alternate in size with two different exchange interactions J and J'. (b) Temperature dependence of the magnetic susceptibility of $LiGaCr_4O_8$ (open circles) and $LiInCr_4O_8$ (full squares) samples measured in an external field of 1 T. (c) Inverse magnetic susceptibility plotted together with Curie-Weiss fits (solid lines).

turn is due to a small Curie contribution from orphan spins. The concentration of defects or impurities is estimated to 2.8 % for A=In, while it becomes negligible for A=Ga with 0.3 %. $\chi(T)$ of the Ga compound shows a flat-like maximum at around 50 K, reminiscent of the uniform spinel oxide $ZnCr_2O_4$[23]. As evident from the inverse of $\chi(T)$ plotted in Fig. 1(c), for temperatures above 120 K $\chi(T)$ follows the Curie-Weiss law of $\chi(T) = C/(T - \Theta_{CW})$ where C is the Curie constant and Θ_{CW} is the Curie-Weiss temperature. The Curie-Weiss fits yield $C=$ 1.97(3) emu·K·mol^{-1} and $\Theta_{CW}=-610(9)$ K for A=Ga and $C = 1.83(2)$ emu·K·mol^{-1} and $\Theta_{CW} = -326(6)$ K for A=In. The effective magnetic moments are evaluated to $\mu_{eff} = 3.96(9)$ μ_B for the Ga compound and $\mu_{eff} = 3.82(9)$ μ_B for the In compound. These are close to the spin-only value of $\mu_{theo} = 3.872\,\mu_B$ and are consistent with the values reported in the previous result[13].

B.   Dielectric constant

The frequency and temperature dependence of the dielectric constant was measured as ranging from 1 kHz to 20 kHz for $LiACr_4O_8$. The measurement results are presented in
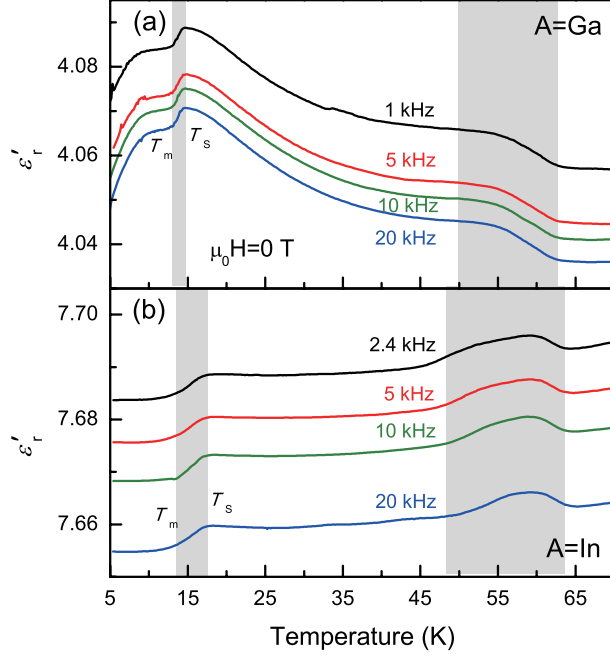
FIG. 2: (Color online) Real part of relative dielectric constant of (a) $LiGaCr_4O_8$ and (b) $LiInCr_4O_8$ measured at zero magnetic field as a function of temperature and frequency. The shaded areas indicate two dielectric anomalies: the magnetostructural phase transition at T_S and the ensuing magnetic transition at T_m together with the magnetodielectric anomaly occurring at about 60 K.

Fig. 2. As indicated by the shaded areas, both samples exhibit two distinct magnetodielectric anomalies. With decreasing temperature from 70 K, the dielectric response displays a broad hump at about 60 K and a step-like drop at $T_S = 15.2$ K for A=Ga and 17.6 K for A=In. The higher-T anomaly is linked to the maximum in $\chi(T)$ [see Fig. 1(b)] and is similar to the dielectric dispersion observed in $ZnCr_2O_4$ for temperatures of $12 - 70$ K[24]. This was ascribed to the development of a short-range magnetic order accompanying local lattice distortions well above T_S. In contrast to $ZnCr_2O_4$, the higher-T hump hardly varies with frequency in the measured frequency range. The lack of frequency dependence might be because the applied frequency is not wide enough to cover a MHz range, unlike the case of $ZnCr_2O_4$. The lower-T dielectric anomaly corresponds to the cubic-to-tetragonal structural phase transition. The long-range nature of the magnetostructural transition is confirmed by the frequency independence of the dielectric response. As previously mentioned, a similar dielectric anomaly has been observed in the uniform counterpart $ZnCr_2O_4$. However, a close comparison reveals a difference between $ZnCr_2O_4$ and $LiACr_4O_8$. In $ZnCr_2O_4$, the dielectric

constant jumps sharply at T_S, reflecting the first-order nature of the simultaneous structural and antiferromagnetic transitions through strong magnetoelastic coupling[24–27]. In the case of LiACr$_4$O$_8$, a steplike decrease of the dielectric constant is observed in a finite temperature interval. The onset and end temperatures correspond to T_S and $T_m = 12.9$ K (13.7 K) for A=Ga (In). This confirms that the magnetic transition is detached from the structural transition in the presence of the bond alternation. Remarkably, the temperature separation between the two transitions, $\Delta T = T_S - T_m$, increases from 2.3 K to 3.9 K as A changes from Ga to In. The correlation between ΔT and $1/B_f$ suggests that T_m is determined by the intertetrahedral interaction J', which couples the small tetrahedrons. As such, the bond alternation provides a control parameter for generating the two-step transition absent for the regular pyrochore system.
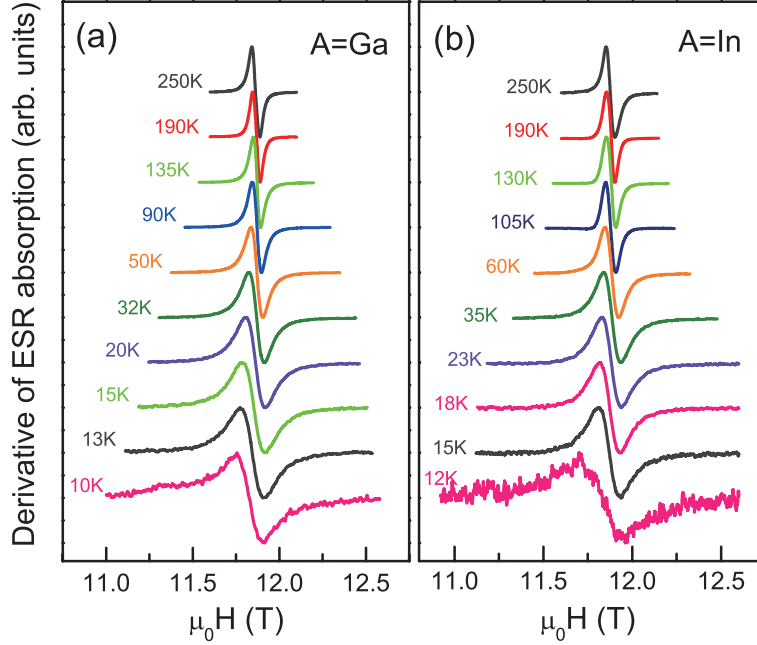
C. Electron spin resonance

FIG. 3: (Color online) Derivative of the ESR absorption spectra of (a) A=Ga and (b) A=In at various temperatures. The spectra are vertically shifted for clarity.

Figure 3 shows the temperature dependence of the high-frequency ESR spectra for LiACr$_4$O$_8$ measured at $\nu = 328.8$ GHz. At room temperature, we observe an exchange-narrowed single Lorentzian line, which originates from paramagnetic Cr$^{3+}(3d^3)$ ions. The

g-factor is evaluated to $g = 1.976(5)$ for both compounds. The obtained g-value, being slightly smaller than a free ion value, is expected for a less than half-filled ion with negligible spin-orbit interaction. The ESR spectra are fitted by a Lorentzian profile and the resulting parameters, the peak-to-peak linewidth (ΔH_{pp}) and the resonance field ($H_{\rm res}$) are plotted in Fig. 4 as a function of temperature. As the temperature is lowered, $\Delta H_{pp}(T)$ initially shows a critical increase and then changes to a weaker T-dependence at T_S and finally reaches drastically below T_m [see Figs. 4(a) and 4(b)]. Over the entire temperature range, the line broadening is well described by a critical power law, $\Delta H_{pp}(T) \propto (T - T_N)^{-p} + A$ (=constant) with the different critical exponent p in three regimes. The multistage evolution of $\Delta H_{pp}(T)$ accompanies the large shift of $H_{\rm res}(T)$ as marked in Figs. 4(c) and 4(d).
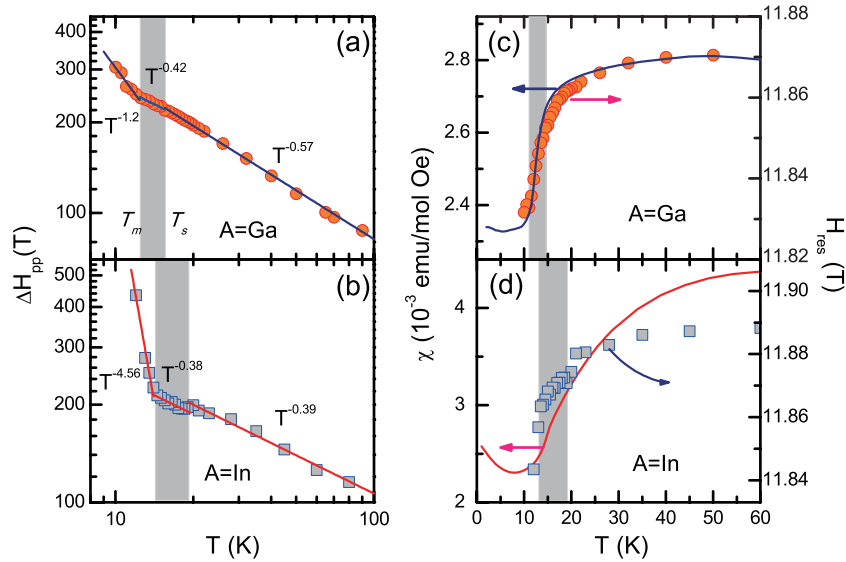

FIG. 4: (Color online) (a) and (b) The peak-to-peak ESR linewidth $\Delta H_{pp}(T)$ vs temperature is plotted for A=Ga and In on a log-log scale. The solid lines are fits to a power law, $\Delta H_{pp}(T) \propto T^{-p}$. The arrows indicate a temperature interval where $\Delta H_{pp}(T)$ changes its exponent p. (c) and (d) Temperature dependence of the resonance field $H_{\rm res}(T)$ for A=Ga and In is shown with the magnetic susceptibility for comparison.

A critical line broadening in a paramagnetic state is a characteristic of frustrated spin systems and is due to the persistence of local spin correlations up to the Curie-Weiss temperature, $\Theta_{\rm CW} \approx 320 - 610\,{\rm K}$[28]. The extracted critical exponent of A=Ga is $p \approx 0.57$, which is quite close to $p \approx 0.56(4)$ observed in the 3D coupled spin tetrahedra $Cu_4Te_5O_{12}Cl_4$[29]. For A=In, this value is reduced to $p \approx 0.39$, being comparable to $p \approx 0.3(9) - 0.4(8)$ re-

8

ported in the distorted triangular antiferromagnet $\alpha-\text{CaCr}_2\text{O}_4$[30]. The smaller p in A=In is a consequence of the reduced dimensionality because of the weak J' interaction and implies that the critical spin fluctuations are suppressed at a paramagnetic state as the strength of the bond alternation increases.

Upon cooling down to the magnetostructural ordering, the exponent in the Ga compound changes from $p = 0.57$ to 0.42 at $T_S = 15.6$ K and then to 1.2 at $T_m = 12.7$ K. The In compound shows a slight change of p and a small drop of $\Delta H_{pp}(T)$ through $T_S = 19.3$ K and then a considerably large increase of $p = 0.38$ to 5.46 at $T_m = 13.8$ K. From the weak anomaly of A=In at T_S, we infer that the spin correlations of the In compound experience a weak change through the structural transition, thereby resulting in a weak magnetostructural coupling. This is supported by a recent neutron diffraction study, which shows the appearance of a weak (201) Bragg peak at T_S[22]. In contrast, the Ga compound undergoes a substantial change of $\Delta H_{pp}(T)$ and thus a strong variation of the spin correlations through T_S, confirming the strong magnetic order precipitated by the structural transition.

In an antiferromagnetically ordered state we would normally expect antiferromagnetic resonance (AFMR) modes, which arise from spin wave excitations by a microwave at $Q = 0, \pm q_{\text{ICM}}$. The anticipated AFMR modes cannot be detected in the employed frequency and field range ($\nu = 200 - 330$ GHz and $\mu_0 H = 0 - 14$ T). This could be due either to a large gap of spin waves or to strong quantum fluctuations, as observed in $\text{CuTe}_2\text{O}_5\text{Br}_2$[31–35]. Instead, the paramagnetic signal persists to the ordered state and disappears at a few degrees below T_m. This suggests that fast fluctuating spins are present in the ordered phase. According to a recent high-resolution neutron diffraction study[16], the minority cubic and majority tetragonal phases coexist below T_S, while the spin-spin correlation length remains small. On this ground, the ESR signal observed below T_S is assigned to the cubic paramagnetic state. For temperatures below T_m, the In compound displays a stronger T-dependence of ΔH_{pp} than the Ga compound [compare Figs. 4(a) and 4(b)]. Accordingly, the In compound has a shorter spin-spin correlation length than the Ga compound.

Before proceeding, we point out that $T < 60$ K $H_{\text{res}}(T)$ matches well with $\chi(T)$ for A=Ga as shown in Fig. 4(c). This is not the case for A=In, in which $H_{\text{res}}(T)$ substantially deviates from $\chi(T)$ above 25 K [see Fig. 4(d)]. As $H_{\text{res}}(T)$ is associated with a buildup of an internal magnetic field, the parallel between $H_{\text{res}}(T)$ and $\chi(T)$ in A=Ga means that the magnetic susceptibility diminishes proportional to the increasing local staggered field formed by the

short-range antiferromagnetic ordering. This is no longer valid for the In compound where singlet fluctuations are dominant.
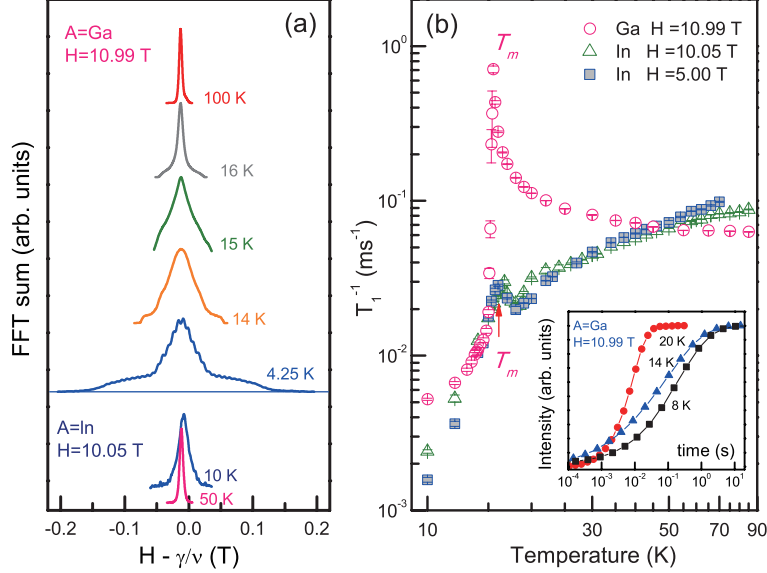
D. ^{7}Li Nuclear spin resonance

FIG. 5: (Color online) (a) Representative ^{7}Li NMR FFT spectra of LiACr$_4$O$_8$ (A=Ga and In). The vertical scale is normalized by the peak height. (b) ^{7}Li nuclear spin-lattice relaxation rate $1/T_1$ on a log-log scale measured at $\mu_0 H = 10.99$ T for A=Ga (open circles) and at $\mu_0 H = 5.00$ T (full squares) and 10.05 T for A=In (open triangles). The inset shows a plot of the recovery curves of A=Ga vs. time at $T = 8$, 14, and 20 K.

In Fig. 5(a), we present the ^{7}Li NMR spectra of LiACr$_4$O$_8$ obtained by monitoring the FFT sum of a spin echo. In the paramagnetic state, the NMR spectra have a narrow single line with no quadrupole splitting as expected from the cubic symmetry at the ^{7}Li site. As $T \longrightarrow T_m$, the widths of the NMR spectra of the In compound increase gradually. In the Ga compound, upon cooling down through T_S, a broad line increases progressively while a narrow paramagnetic line diminishes. This is related to the growing volume fraction of the tetragonal phase against the strained cubic phase below T_S[16]. In the ordered state, the spectrum consists of both a relatively narrow line and a broad line, being consistent with the previous result[14]. In contrast to Ref.[14], however, we find no clear signature of a first-order transition between T_m and T_S. This assertion is based on the fact that the recovery curves

of the spin-echo intensity vs. time are described by a single stretched-exponential function, say at $T = 14$ K, with no hint of an additional relaxation function [see inset of Fig. 5(b)]. Furthermore, our NMR spectrum contains no sharp paramagnetic signal on top of the broad structured spectrum [compare Fig. 3(a) in Ref. 14 to Fig. 5(a)]. This discrepancy could be caused by extrinsic effects such as defects or a difference in the magnetic field applied between the two experiments since the width of the paramagnetic signal is severely increased at our applied field of 10.99 T.

We now discuss the T-dependence of the nuclear spin-lattice relaxation rate $1/T_1$ and spin-spin relaxation rate $1/T_2$. As shown in Fig. 5(b), $1/T_1$ of the Ga sample increases steeply with decreasing temperature. Both $1/T_1$ and $1/T_2$ show a divergence at $T_m = 15.4$ K due to a slowing down of the Cr spin fluctuations [see also Fig. 6(a)]. This clearly demonstrates a second order phase transition to long-range magnetic order. The critical relaxation rate is given by $1/(T_1 T) \propto \sum_q A^2(q) \chi''(q, \omega_0)$ with the hyperfine form factor $A(q)$, the nuclear Larmor frequency ω_0, and the dynamic susceptibility χ''. In the paramagnetic state, our data are described by a single power law $1/(T_1 T) \propto (T - T_m)^{-\alpha}$ with the critical exponent $\alpha = 0.5(5)$ as shown in Fig. 6(b). This value is close to $\alpha = 0.5$, expected for 3D fluctuations of local antiferromagnetic moments[36].

We now consider $1/T_1$ and $1/T_2$ of the In compound. As the temperature is reduced, $1/T_1$ first decreases exponentially with a slope change at $T^* = 20.1$ K, and then shows an upturn at $T_S = 16.5$ K, a subsequent small peak at $T_m = 15.7$ K, and finally a power-law-like decrease in the ordered state [see Fig. 6(c)]. The same successive anomalies are identified in the T-dependence of $1/T_2$ as plotted in Fig. 6(a). $1/T_2$ starts to decrease around T^*, then shows an upturn at T_S, and finally increases gradually with a very small kink at T_m. In the paramagnetic state, the exponential decrease of $1/T_1$ indicates the opening of a spin gap.

To examine the thermal activation behavior, $1/T_1$ is plotted against $1/T$ in Fig. 6(c). For temperatures above 25 K (below 0.04 K^{-1}), all the data are well fitted by an Arrhenius form $1/T_1 \propto \exp(-\Delta(H)/T)$, yielding the H-dependent spin gap $\Delta(H)$ (solid lines). The extracted spin gap $\Delta(H)$ vs H is plotted in Fig. 6(d). The zero-field gap is estimated to be $\Delta(0) = 23$ K. The extracted gap is somewhat smaller than $\Delta = 31$ K obtained from a previous ^{7}Li NMR study[14]. This discrepancy is largely due to the different temperature and field windows chosen to evaluate the spin gap. The spin gap behavior suggests that singlet fluctuations govern spin dynamics at elevated temperatures. The T^* anomaly, clearly visible
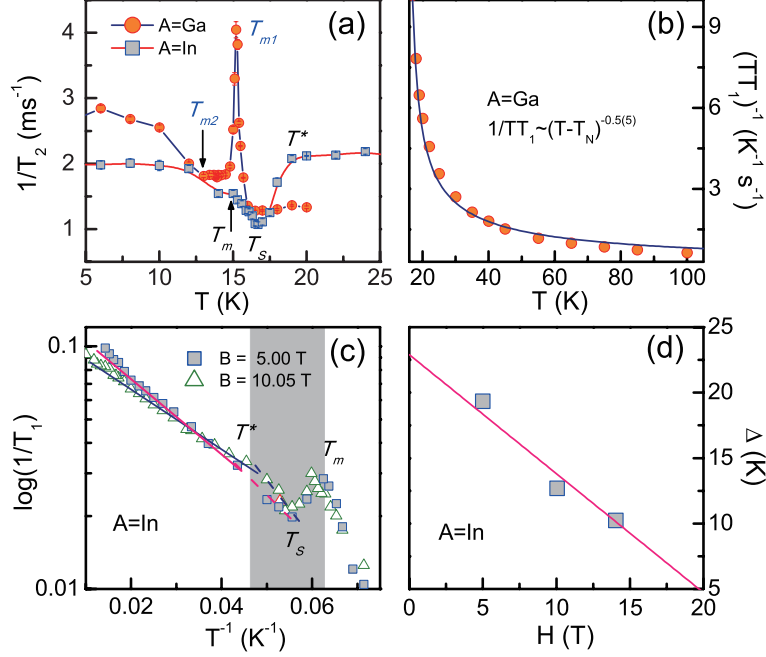
FIG. 6: (Color online) (a) Nuclear spin-spin relaxation rate $1/T_2$ measured at $\mu_0 H = 10.99$ T for A=Ga (full circles) and 10.05 T for A=In (full squares). (b) $(T_1 T)^{-1}$ vs temperature for A=Ga. The solid line is a fit to the equation $(T_1 T)^{-1} \propto (T - T_m)^{-\alpha}$. (c) $\log(1/T_1)$ vs inverse temperature measured at $\mu_0 H = 5.00$ T (full squares) and 10.05 T (open triangles) for A=In. The solid lines are fits to an activation behavior and the dashed lines are guide to the eyes to indicate a change of a spin gap. (d) Spin gap $\Delta(H)$ vs temperature.

in $1/T_1$ and $1/T_2$, is ascribed to a thermal crossover from a tetramer singlet to a correlated paramagnetic state (see below for further discussion).

E.   Muon spin resonance

To further investigate the evolution of spin correlations, we performed μSR measurements. Figures 7(a) and 7(c) show the muon polarization of LiACr$_4$O$_8$ taken at ISIS. In the paramagnetic state, the μSR spectrum is typical for a slow relaxation. As the temperature is reduced from 25 K, the initial asymmetry drops rapidly through T_m [see also Fig. 8(a)]. The missing asymmetry is associated with magnetic ordering, giving rise to an unresolved precession signal within the ISIS muon beam time window. In searching for the oscillating muon signal, we resort to the LAMPF spectrometer at TRIUMF, offering a continuous muon
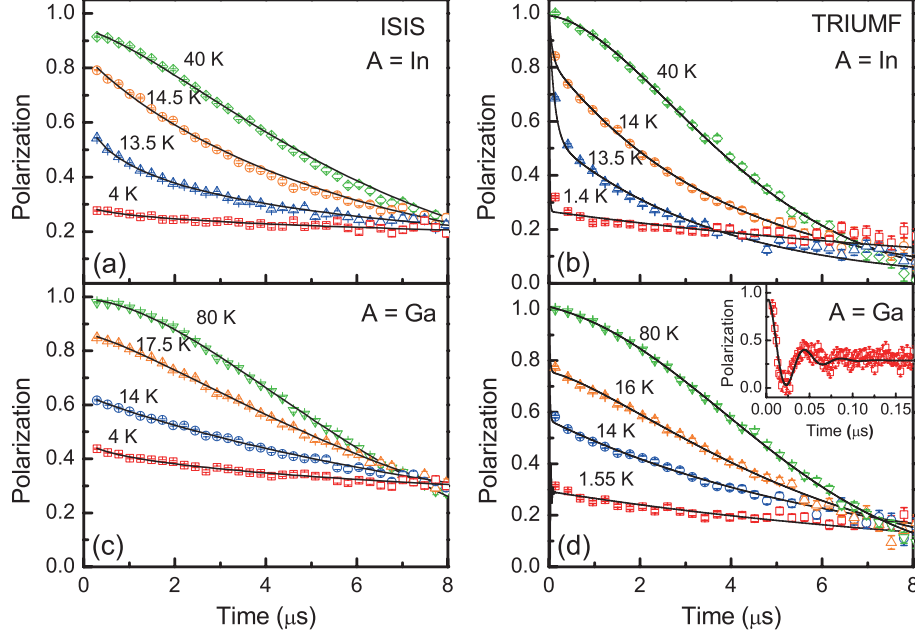
FIG. 7: (Color online) (a) and (c) Temperature dependence of μSR spectra taken at ISIS for LiInCr$_4$O$_8$ and LiGaCr$_4$O$_8$ at various temperatures, respectively. (b) and (d) Temperature dependence of μSR spectra recorded at TRIUMF for LiInCr$_4$O$_8$ and LiGaCr$_4$O$_8$ at various temperatures, respectively. The solid black lines represent fits to the data as described in the text. The inset of (d) shows the oscillation signal of LiGaCr$_4$O$_8$ for the first 0.17 μs.

source with a better time resolution. Overall, the CW and pulse μSR spectra look alike. In the case of the In sample, we failed to detect a fast precession signal below T_m, whereas in the Ga sample, we observed a spontaneous oscillation for the first 0.17 μs [see the inset of Fig. 7(d)]. This suggests that in the ordered state of the In sample, a local internal magnetic field at the muon site is still dynamic on a microsecond timescale. We further note that the oscillation is more heavily damped in LiGaCr$_4$O$_8$ than ZnCr$_2$O$_4$[37]. This implies that the breathing pyrochlore LiACr$_4$O$_8$ compounds have a much stronger dynamical spin component in the ordered state than the uniform ZnCr$_2$O$_4$.

The muon spectra of both compounds are fitted to a sum of a simple exponential function multiplied by a cosine function and a stretched exponential function, $P_z(\mathrm{t}) = P_{\mathrm{fast}}e^{-\lambda_f t}\cos(2\pi f_\mu t + \phi) + P_{\mathrm{slow}}e^{(-\lambda_s t)^{\beta_s}}$. λ_f and λ_s denote the muon relaxation rates of the respective fast and slow relaxation component. The obtained fit parameters are summarized in Fig. 8. The exponent gradually decreases with temperature from $\beta_s = 2$ (a Gaussian-like shape), reaching $\beta_s = 1$ (simple exponential function) below T_m. This again confirms the existence
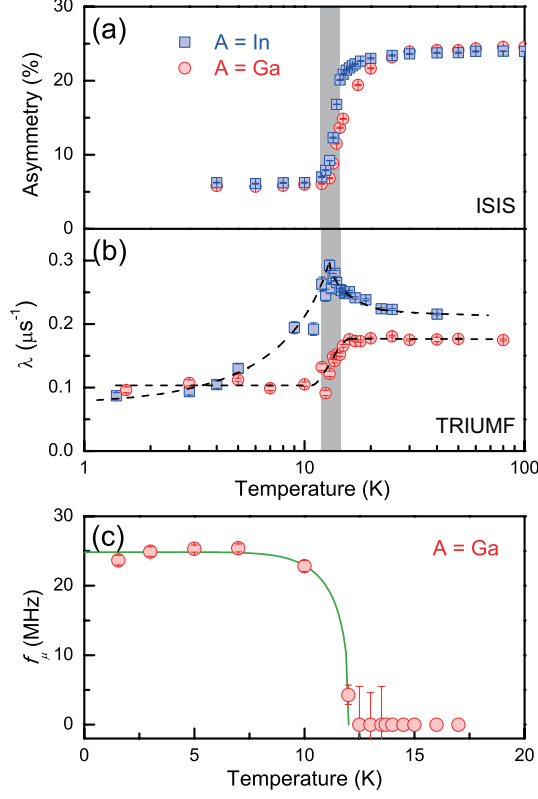
13

FIG. 8: (Color online) (a) Temperature dependence of the initial asymmetry of $LiACr_4O_8$ extracted from the μSR spectra taken at ISIS. (b) Muon relaxation rate λ_s of $LiACr_4O_8$ as a function of temperature, obtained from the μSR spectra recorded at TRIUMF. The shaded region denotes the magnetic ordering. (c) Temperature dependence of the muon-spin-precession frequency f_μ. The solid green line is a fit to Eq. (2).

of a substantial dynamical spin fluctuation in the ordered state. As evident from the semi-log plot of Fig. 8(b), the slow muon relaxation rate of the In compound shows a clear λ-like peak at $T_m = 13.1$ K. The relaxation rate of the Ga compound undergoes a step-like decrease at $T_S = 15.8$ K, being independent of temperature in both the paramagnetic and the ordered side.

From the precession signal, we can deduce the internal field and thus the temperature dependence of the order parameter. The extracted frequency as a function of temperature is fitted to the phenomenological function,

$$f_\mu(T) = f_\mu(0)(1 - (T/T_m)^\alpha)^\beta \qquad (2)$$

where $f_\mu(0)$ denotes the initial frequency at $T = 0$. A fit to Eq. (2) allows the critical

14

TABLE I: Temperatures of magnetic and structural transitions of LiACr$_4$O$_8$ determined using different experimental techniques.

A	Dielectric constant	ESR	NMR	μSR
Ga	$T_S = 15.2$ K	$T_S = 15.6$ K	$T_S = 15.4$ K	$T_S = 15.8$ K
	$T_m = 12.9$ K	$T_m = 12.7$ K	$T_m = 12.9$ K	$T_m = 12.01$ K
In	$T_S = 17.6$ K	$T_S = 19.3$ K	$T_S = 16.8$ K	-
	$T_m = 13.7$ K	$T_m = 13.8$ K	$T_m = 15.7$ K	$T_m = 13.1$ K

temperature and the critical exponent β to be extracted. Typically, the critical exponent β varies with the choice of T_m. The best fit yields $f_\mu = 24.7(4)$ MHz, $\alpha = 8.2(6)$, and $\beta = 0.35(8)$ with a fixed value of $T_m = 12.01$ K. We note that the spontaneous oscillation is no longer detectable above T_m since the local internal magnetic field fluctuates faster than a MHz time scale between T_m and T_S. The value of the critical exponent is expected for a 3D Heisenberg antiferromagnet. The obtained frequency is close to that found in ZnCr$_2$O$_4$[37], corresponding to the internal magnetic field of 0.183 T. However, $\beta = 0.20(1)$ of ZnCr$_2$O$_4$ is much smaller than that of LiGaCr$_4$O$_8$.

IV. DISCUSSION AND SUMMARY

Multiple resonance techniques adopted to investigate the full aspect of magnetic correlations in LiGaCr$_4$O$_8$ enable further understanding of the two-stage transition, which is in sharp contrast to the single transition in the uniform pyrochlore ZnCr$_2$O$_4$.

In Table I, we list the magnetic and structural ordering temperatures determined by dielectric constant, ESR, ^{7}Li NMR and μSR measurements. It should be noted that the dielectric constant and ESR are capable of probing the structural and magnetic transition, whereas NMR and μSR are rather insensitive to the structural transition. The key finding of this work is that the multistage symmetry breaking processes depend on a degree of bond alternation.

First, we emphasize that LiACr$_4$O$_8$ features a second-order magnetic transition. Since the spin-lattice coupling alone in ZnCr$_2$O$_4$ leads to the first-order magnetostructural transition, the breathing lattice distortion is regarded as a key ingredient for the second-order transition.

The magnetoelastic coupling combined with bond alternation changes the character of the magnetic transition and creates the multiple dielectric anomalies. The two-stage transition is associated with the two different magnetoelastic couplings of the S- and L-tetrahedra. We recall that the 60 K dielectric anomaly is lacking in $ZnCr_2O_4$ (see Fig. 2). The alternating tetrahedra are expected to induce stronger ionic displacements than the regular tetrahedra since the small and large tetrahedra will build disparate local lattice distortions proportional to their exchange interaction energy. With increasing bond alternation, the ordered moments become more dynamic. According to the μSR data, the spontaneous muon precession seen in A=Ga is no longer detectable in A=In. In addition, the paramagnetic ESR signal persists below T_m. These observations indicate that both microsecond and nanosecond spin dynamics are present in the ordered state. This is fully consistent with the neutron diffraction results which show the coexistence of the strained cubic and tetragonal phases with a short spin-spin correlation length below T_m[16].

Second, we differentiate the multistage symmetry breaking process between $LiGaCr_4O_8$ and $LiInCr_4O_8$. As summarized in Table I, the spin-lattice coupling drives the Ga compound to the cubic-to-tetragonal transition at $T_S = 15.2 - 15.8$ K. This accompanies the second-order antiferromagnetic ordering as evidenced by the ^{7}Li NMR and μSR data. At a few kelvins below T_S, the second magnetic order ensues with new magnetic propagation vectors[22]. Considering the In compound, the magnetic ordering has only a weak signature at $T_S = 17.6 - 19.3$ K. The λ-like anomaly seen by ^{7}Li and μSR occurs at $T_m = 13.1 - 13.7$ K. It is worth mentioning that T_m obtained from ^{7}Li NMR is a few kelvins higher than that from other experimental techniques. This inconsistency is not merely experimental. A similar incompatibility of T_m has been observed in the coupled spin tetrahedral system $Cu_2Te_2O_5Br_2$, which shows spin singlet correlations in a paramagnetic state and, subsequently, undergoes magnetic ordering at T_N=11.4 K[34]. The proximity to a quantum critical point was discussed as a possible origin. In the same way, the structural transition temperature T_S determined by the dielectric constant and ESR is higher than $T_S = 16$ K obtained by the specific heat. This is ascribed to a temporal distribution of lattice distortions.

Next, we rationalize an intriguing symmetry breaking process of the In compound. At high temperatures, $T >> J'$ single tetrahedron correlations dominate. This is inferred from the activation behavior of $1/T_1$, originating from the formation of tetramer singlets with a spin gap of an order of J. When J' is switched on, the tetramer singlets can be broken

into two dimer singlets[38] or hexagonal plaquettes[39]. In this situation, a thermal crossover is anticipated to occur at $T \sim J'$ from the isolated tetramer singlet to the dimer singlet or correlated paramagnet. The slope change in $1/T_1$ and the drop in $1/T_2$ at $T^* = 20.1$ K may be an experimental indication of the thermally driven transition. This scenario is supported by the observation that the inelastic magnetic mode softens above T_S[16]. We further note that soft singlet modes have been reported in the frustrated spin-ladder $BiCu_2PO_6$, which borders a phase boundary between a columnar dimer and a resonating valence bond[40].

The thermally induced symmetry reduction only partly relieves frustration and hence the tetragonal compression cannot give a strong impetus to the formation of the magnetically ordered state. Rather, nonmagnetic singlet or correlated paramagnetic fluctuations prevail over the ordered moments in a temperature between T_S and T_m where the majority tetragonal and the minority cubic phases coexist. Compared to the Ga compound, the structural transition thus accompanies a weak magnetic ordering[22]. Upon cooling down through T_m, the volume fraction of the tetragonal phase increases, so that the strength of the long-range magnetic order increases against the singlet fluctuations. For the case of the Ga compound, the bond alternation is not sufficient to drive a highly correlated paramagnetic state to a singlet state. As a consequence, the spin-lattice coupling is a unique route to relieve the degeneracy, leading to a strong union of the magnetic and structural transitions.

In summary, we characterized multistage symmetry lowering processes in $LiACr_4O_8$ using various magnetic resonance techniques. We find that structural and magnetic transitions are weakly coupled in the In compound, having a sufficiently strong bond alternation. This is related to a partial lift of degeneracy through a thermal crossover from tetramer to dimer singlets or correlated paramagnets proceeding the structural transition. The Ga compound with moderate bond alternation has a highly correlated paramagnetic state, as does the uniform pyrochlore counterpart $ZnCr_2O_4$. The anticipated structural and magnetic transitions occur simultaneously, demonstrating that exactly the same magnetoelastic mechanism is applied to both $LiGaCr_4O_8$ and $ZnCr_2O_4$. However, the number and nature of the magnetic transition differ. The two successive magnetic transitions of a second-order character in $LiGaCr_4O_8$ highlights an intriguing role of breathing distortions in determining magnetic phases and correlations. Thus, $LiACr_4O_8$ offers an excellent foundation for understanding the symmetry breaking process in frustrated spin systems with bond alternation and spin-lattice coupling

Acknowledgements

_____

* `kchoi@cau.ac.kr`

[1] See, for example, H. T. Diep, *Magnetic Systems with Competing Interactions* (Singapore: World Scientific, 1994).

[2] J. E. Greedan, J. Mater. Chem. **11**, 37 (2001); R. Moessner and A. P. Ramirez, Phys. Today **59**, 24 (2006).

[3] See for review, S.-H. Lee, H. Takagi, D. Louca, M. Matsuda, S. Ji, H. Ueda, Y. Ueda, T. Katsufuji, J.-H. Chung, S. Park, S.-W. Cheong, and C. Broholm, J. Phys. Soc. Jpn. **79**, 011004 (2010).

[4] P. W. Anderson, Phys. Rev. **102**, 1008 (1956).

[5] S. T. Bramwell and M. J. P. Gingras: Science **294**, 1495 (2001).

[6] S.-H. Lee, C. Broholm, W. Ratcliff, G. Gasparovic, Q. Huang, T. H. Kim, and S.-W. Cheong, Nature **418** 856, (2002).

[7] J. Villain, Z. Phys. B: Condens. Matter **33**, 31 (1979).

[8] R.R. Spobral, C. Lacroix, and R.R. Sobral, Solid State Comm., **103**, 407 (1997).

[9] Y. Yamashita and K. Ueda, Phys. Rev. Lett. **85**, 4960, (2000).

[10] O. Tchernyshyov, R. Moessner, and S. L. Sondhi, Phys. Rev. Lett. **88**, 067203 (2002).

[11] H. Tsunetsugu, J. Phys. Soc. Jpn. **70**, 640 (2001).

[12] M. E. Zhitomirsky, Phys. Rev. Lett. **88**, 057204 (2002).

[13] Y. Okamoto, G. J. Nilsen, J. P. Attfield, and Z. Hiroi, Phys. Rev. Lett. **110**, 097203 (2013).

[14] Y. Tanaka, M. Yoshida, M. Takigawa, Y. Okamoto and Z. Hiroi, Phys. Rev. Lett. **113**, 227204 (2014).

[15] Y. Okamoto, G. J. Nilsen, T. Nakazono and Z. Hiroi, J. Phys. Soc. Jpn. **84**, 043707 (2015).

[16] G. J. Nilsen, Y. Okamoto,, T. Masuda, J. Rodriguez-Carvajal, H. Mutka, T. Hansen, and Z.

Hiroi, Phys. Rev. B **91**, 174435 (2015).

[17] K. Kimura, S. Nakatsuji and T. Kimura, Phys. Rev. B **90**, 060414(R), (2014).

[18] O. Benton and Nic Shannon, J. Phys. Soc. Jpn. **84**, 104710 (2015).

[19] L. Savary, H.-Y. Kee, Y. B. Kim, and G. Chen, arXiv:1511.06972 (2015).

[20] B. Canals and C. Lacroix, Phys. Rev. Lett. **80**, 2933 (1998); B. Canals and C. Lacroix, Phys. Rev. B **61**, 1149 (2000).

[21] R. Moessner and J. T. Chalker, Phys. Rev. Lett. **80**, 2929 (1998).

[22] According to a priviate communication by S. Ji, a weak magnetic Bragg peak appears at the structural transition temperature in $LiInCr_4O_8$, confirming the magnetostructural nature of a higher-temperature transition at T_S. Noticeably, the magnetic peak was not resolved in the earlier neutron diffraction study[16].

[23] H. Ueda, H. A. Katori, H. Mitamura, T. Goto, and H. Takagi, Phys. Rev. Lett. **94**, 047202 (2005).

[24] I. Kagomiya, K. Kohn, M. Toki, Y. Hata, and E. Kita, J. Phys. Soc. Jpn. **71**, 916 (2002).

[25] J.-H. Chung, M. Matsuda, S.-H. Lee, K. Kakurai, H. Ueda, T. J. Sato, H. Takagi, K.-P. Hong, and S. Park: Phys. Rev. Lett. **95**, 247204 (2005).

[26] H. Ueda, H. Mitamura, T. Goto, and Y. Ueda: Phys. Rev. B **73**, 094415 (2006).

[27] S. Ji, S.-H. Lee, C. Broholm, T. Y. Koo, W. Ratcliff, S.-W. Cheong, and P. Zschack: Phys. Rev. Lett. **103**, 037201 (2009).

[28] S.-H. Lee, C. Broholm, T. H. Kim, W. Ratcliff, and S.-W. Cheong, Phys. Rev. Lett. **84**, 3718, (2000).

[29] K.-Y. Choi, S. H. Do, P. Lemmens, J. van Tol, J. Shin, G. S. Jeon, Y. Skourski, J.-S. Rhyee, and H. Berger, Phys. Rev. B **90**, 184402 (2014).

[30] D. Wulferding, K.-Y. Choi, P. Lemmens, A. N. Ponomaryov, J. van Tol, A. T. M. Nazmul Islam, S. Toth, and B. Lake, J. Phys.: Condens. Matter **24** (2012).

[31] P. Lemmens, K.-Y. Choi, E. E. Kaul, C. Geibel, K. Becker, W. Brenig, R. Valenti, C. Gros, M. Johnsson, P. Millet, and F. Mila, Phys. Rev. Lett. **87**, 227201 (2001).

[32] C. Gros, P. Lemmens, M. Vojta, R. Valenti, K.-Y. Choi, H. Kageyama, Z. Hiroi, N. V. Mushnikov, T. Goto, M. Johnsson, and P. Millet, Phys. Rev. B **67**, 174405 (2003).

[33] K. Prsa, H. M. Rønnow, O. Zaharko, N. B. Christensen, J. Jensen, J. Chang, S. Streule, M. Jiménez-Ruiz, H. Berger, M. Prester, and J. Mesot,, Phys. Rev. Lett. **102**, 177202 (2009).

[34] S.-H. Baek, K.-Y. Choi, H. Berger, B. Büchner, and H.-J. Grafe, Phys. Rev. B **86**, 180405 (2012).

[35] T. Besara, E. S. Choi, K.-Y. Choi, P. L. Kuhns, A. P. Reyes, P. Lemmens, H. Berger, and N. S. Dalal, Phys. Rev. B **90**, 054418 (2014).

[36] T. Moriya and K. Ueda, Solid State Commun. **15**, 169 (1974).

[37] I. M. Marshall, S. J. Blundell, F. L. Pratt, A. Husmann, C. A. Steer, A. I. Coldea, W. Hayes, and R. C. C. Ward, J. Phys.: Condens. Matter **14**, L157 (2002).

[38] A. J. Garcia-Adeva and D. L. Huber, Phys. Rev. Lett. **85**, 4598 (2000).

[39] Michael Hermele, Matthew P. A. Fisher, and Leon Balents, Phys. Rev. B **69**, 064404 (2004).

[40] K.-Y. Choi, J.W. Hwang, P. Lemmens, D. Wulferding, G. J. Shu, and F. C. Chou, Phys. Rev. Lett. **110**, 117204 (2013).